Journal of Iron and Steel Research, International 24 (2017) 1199—1205

Contents lists available at ScienceDirect

Journal of Iron and Steel Research, International

journal homepage: www.chinamet.cn

Influence of laser re-melting and vacuum heat treatment on plasma-sprayed FeCoCrNiAl alloy coatings

Dan-yang Lin[1], Nan-nan Zhang[1,*], Bin He[1,2], Bing-qian Jin[1], Yue Zhang[1], De-yuan Li[1], Fu-yu Dong[1]

[1] Department of Material Science and Engineering, Shenyang University of Technology, Shenyang 110870, Liaoning, China

[2] Department of Pipeline, Shenyang Institute of Special Equipment Inspection & Research, Shenyang 110032, Liaoning, China

ARTICLE INFO

Key words:
Plasma spray
High entropy alloy
Vacuum heat treatment
Laser re-melting
FeCoCrNiAl alloy coating

ABSTRACT

FeCoCrNiAl high entropy alloy coatings were prepared by supersonic air-plasma spraying. The coatings were post-treated by vacuum heat treatment at 600 and 900 ℃, and laser re-melting with 300 W, respectively, to study the influence of different treatments on the structure and properties of the coatings. The phase constitution, microstructure and microhardness of the coatings after treatments were investigated using X-ray diffraction, scanning electron microscopy and energy dispersive spectrometry. Results showed that the as-sprayed coatings consisted of pure metal and Fe-Cr. The $AlNi_3$ phase was obtained after the vacuum heat treatment process. A body-centered cubic structure with less $AlNi_3$ could be found in the coating after the laser re-melting process. The average hardness values of the as-sprayed coating and the coatings with two different temperature vacuum heat treatments and with laser re-melting were 177, 227, 266 and 682 HV, respectively. This suggests that the vacuum heat treatment promoted the alloying process of the coatings, and contributed to the enhancement of the coating wear resistance. The laser re-melted coating showed the best wear resistance.

1. Introduction

Yeh[1,2] first proposed the concept of high entropy alloys (HEAs) in 1995. Typically, HEAs consist of five or more, but less than 13, principal elements. The component of each element should be between 5% and 35%, and the character of HEAs is determined by the combined features of multiple elements[3,4]. For distinguishing HEAs and traditional alloys, the number of principal elements was defined as more than five. In a similar fashion, alloys with one principal element are considered as low entropy alloys. Middle entropy alloys are between these two kinds of alloys and commonly have two to four principal elements[5].

The structure of HEAs is unique and no complex intermetallic compound exists within it due to the high entropy in the alloy system. Thus, simple solid solutions, like body-centered cubic (BCC), face-centered cubic (FCC) and even hexagonal close-packed (HCP) structures, as proved recently, tend to form[6]. The high solid solubility or single phase contributes to the potential characters of HEAs[7-9], including high strength and hardness, good wear, heat[10] and corrosion resistance, good magnetism performance and even bulk metallic glass properties[11].

HEAs have wide application prospects as a result of their outstanding properties[12]. They are even considered as potential nuclear materials[13]. Therefore, the utilization of HEAs in the preparation of coatings is a vital orientation for their development.

The current most common method for preparing HEA coatings is using laser cladding, which has many advantages. For instance, the coatings after laser cladding have uniform microstructures and a strong combination with the substrate[14-16]. However, laser cladding provides a lower efficiency due to the small spot size and slow scanning speed. Furthermore, the thermal injection of laser cladding is so high that it usually produces deformations, grain growth and phase changes to the workpiece after several claddings, which can have a detrimental effect on the qualities of the workpieces. In addition, physical vapor deposition (PVD), like magnetron sputtering and electron-beam evaporation deposition, is also used to prepare HEA coatings, since

* Corresponding author. Ph.D.
E-mail address: *zhangnn@sut.edu.cn* (*N.N. Zhang*).

Received 21 December 2016; Received in revised form 14 March 2017; Accepted 22 March 2017
Available online 15 December 2017

the coating thickness can be well controlled. However, there are some drawbacks for PVD. The long production cycle time and expensive price have restricted its development. Thus, finding a new technology for the preparation of HEA coatings is a vital research interest.

Nowadays, plasma spraying is one of the most commonly used technologies for preparing coatings[17,18]. It is a kind of thermal spray technology that uses high temperature plasma as its heat source and is mainly used to spray powder. Typically, heat treatment or re-melting is required to achieve a high quality coating after the plasma spray process. Furthermore, the efficiency of plasma spray deposition is much higher than other methods and every corner of the workpiece can be reached.

Thus, in this study, a plasma spray method combined with vacuum heat treatment and laser re-melting was used to prepare FeCoCrNiAl[19] HEA coatings.

2. Experimental Procedure

A 304 stainless steel was used in this experiment, and Fe, Co, Cr, Ni and Al powders of around 48 μm with more than 99% purity were mixed together at the same molar ratio. A planetary ball mill was used to mix the powders for 8 h. The ball material ratio (mass ratio) was 10∶1 and the revolution rate was 200 r/min. A supersonic atmospheric plasma spraying system (3710 Praxair, USA) was used to spray the mixed powder at 500 A and 40 V. Part of the as-sprayed samples were heated in a high temperature vacuum tube (CVD, Hefei, China) for 10 h at 100 Pa. The other samples were re-melted using a semiconductor laser (FL-Dlight-1500, Xi′an, China) with a 300 W power, 3 mm×1 mm spot size and 3 mm/s scanning speed. The wear resistance of the coatings was tested using a universal wear tester (MMW-1) with a disk made of Cr12MoV as the counterpart with a 100 N load and a 100 r/min revolution rate for 15 min at room temperature. The structure and elemental distribution of the coatings were observed with a scanning electron microscope (Hitachi-S3400, Japan). The phase composition was analyzed with an X-ray diffractometer (Shimadzu 7000, Japan), with a scanning speed of 8 (°)/s and scan range of 20°－90°. The microhardness of the coatings was tested using a Vickers hardness tester (DHV-1000) with a 1.96 N load and dwell time of 10 s.

3. Results and Discussion

Fig. 1(a) shows the X-ray diffraction pattern of the as-sprayed coating. It can be seen that the as-sprayed coating mainly consists of pure metals, except for small quantities of Fe-Cr and FeO. The coating cannot be deemed a HEA coating, since no high entropy phase was obtained. After 600 and 900 ℃ heat treatment, and laser re-melting, as shown in Fig. 1(b), the composition in the coatings changed. After the 600 ℃ heat treatment, a BCC structure existed in the coating. Cr-O, $AlNi_3$ and pure metals, like Al and Ni, could also be detected. After the 900 ℃ heat treatment, the content of Cr-O increased and the content of pure metal decreased. After laser re-melting, BCC and $AlNi_3$ phases could be

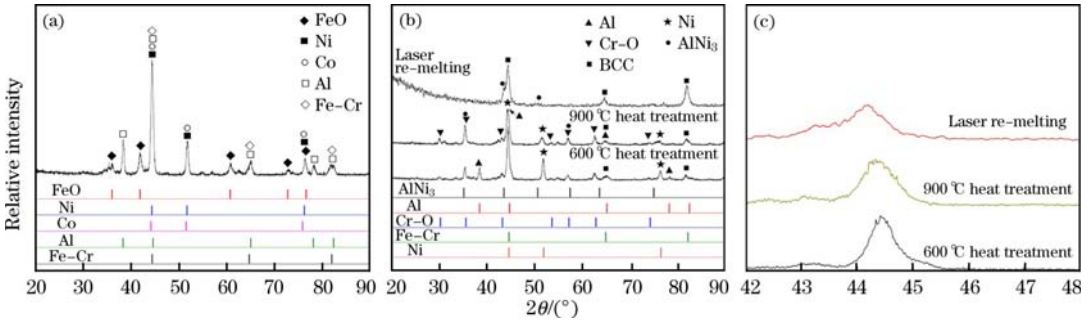

(a) As-sprayed coating; (b) Diffraction angles of 20°－90°; (c) Diffraction angles of 42°－48°.

Fig. 1. X-ray diffraction patterns.

detected, similar to the conclusion of Chen et al.[20].

According to the Gibbs free energy formula[21],

$$\Delta G_{mix}=\Delta H_{mix}-T\Delta S_{mix} \quad (1)$$

where, ΔH_{mix} represents the mixing enthalpy of the alloy system; T represents the thermodynamic temperature; ΔS_{mix} represents the mixing entropy of the alloy system; and ΔG_{mix} represents the Gibbs free energy. According to the Boltzmann entropy hypothesis, the mixing enthalpy of an alloy system can be represented as:

$$\Delta S_{mix}=-R[C_1\ln C_1+C_2\ln C_2+\cdots+C_n\ln C_n] \quad (2)$$

where, R represents the gas constant; and C_1, $C_2\cdots C_n$ represents the mole fraction of each element. The diffusion phenomenon produced by heat treatment enhanced the system entropy according to Eq. (2). It is known that the mixing entropy of an alloy will increase with increasing treatment temperature. The

metallurgical process existed in the process of laser re-melting. Thus, the system entropy of the coatings after laser re-melting reached its highest point.

The increase in system entropy can reduce the free energy of an alloy system, making it difficult to form an intermetallic compound, thereby forming relatively stable simple solid solutions[22]. The elemental diffusion is not sufficient after heat treatment at 600 and 900 ℃; thus, the system entropy is low. For the sample after laser re-melting, the re-melting process fully mixed the elements, which significantly enhanced the entropy of the alloy system. Thus, the free energy of the system markedly decreased, meaning that the formation of intermetallic compounds is restricted to a great extent and now tends towards forming simple solid solutions. However, $AlNi_3$ was detected in the X-ray diffraction patterns, since the free energy of the system is codetermined by ΔH_{mix} and ΔS_{mix}. As can be seen in Table 1[23], the mixing enthalpy of Ni and Al is －22 kJ/mol, which is the lowest among all kinds of combinations in the coating. Thus, $AlNi_3$ can still form while other intermetallic compounds cannot exist with low free energy. However, its formation has already been restricted to a large extent, since the content of $AlNi_3$ was decreased. The solid solubility of atomic Al gradually increased, since the content of $AlNi_3$ decreased, which caused greater lattice distortion. This result is similar to the conclusion of Widom[24]. The atomic radius of Al is larger than the average atomic radius in the solid solution system, which leads to a larger interplanar crystal spacing. According to Bragg's law[25], the diffraction peak shifts to a smaller angle, as shown in Fig. 1(c).

Table 1
Mixing enthalpy between each element (kJ/mol)

Element	Fe	Co	Cr	Ni	Al
Fe	0	—	—	—	—
Co	－1	0	—	—	—
Cr	－1	－4	0	—	
Ni	－2	0	－7	0	—
Al	－11	－19	－10	－22	0

The oxide disappeared because the process of laser re-melting can make it float up to the molten pool surface and fall from the coating[26].

Fig. 2 shows the microstructure of the as-sprayed and vacuum heat-treated coatings. Some splat particles can be observed in Fig. 2(a). It presents the typical characteristic of a thermal sprayed coating[27]. Particles that have not completely been melted are found in Fig. 2(b).

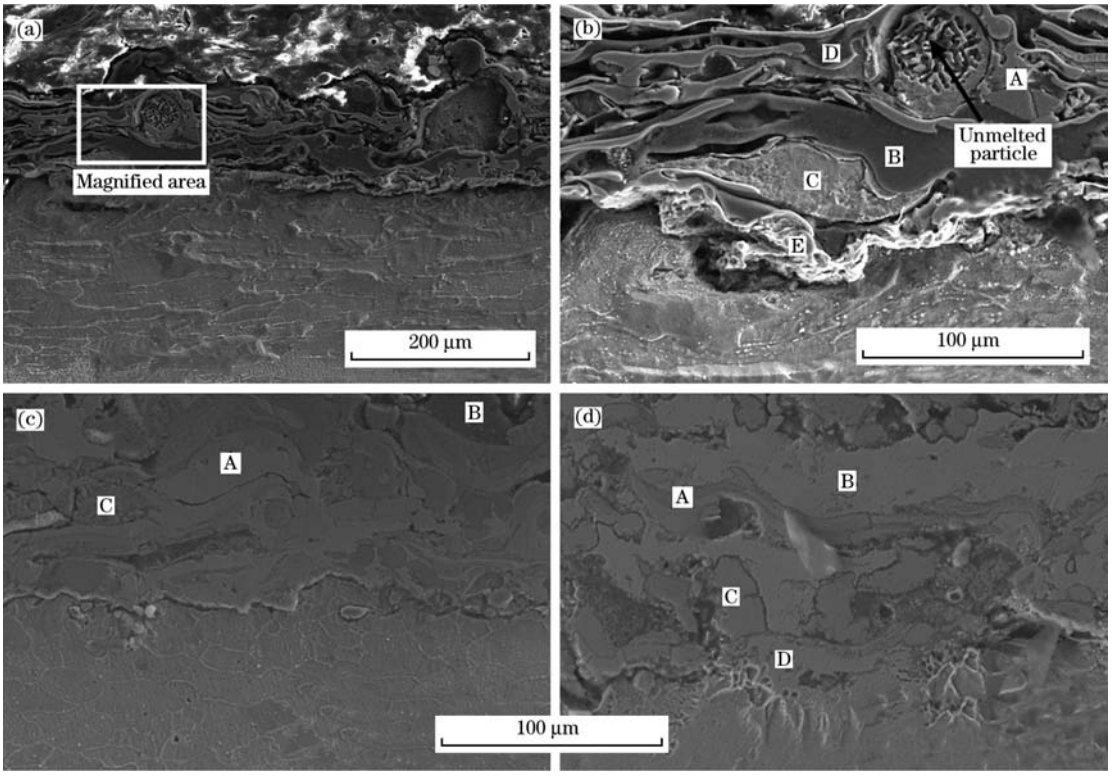

(a) As-sprayed coating; (b) Local enlargement of as-sprayed coating in (a);
(c) Coating after 600 ℃ vacuum heat treatment; (d) Coating after 900 ℃ vacuum heat treatment.

Fig. 2. Cross section of as-sprayed coating and coating after different temperature heat treatments.

Based on the experiments of Munitz et al.[28], a 10 h vacuum heat treatment was done to FeCoCrNiAl coatings. It can be obviously observed in Fig. 1

(c) that the boundary line is not clear and the microstructure becomes more uniform after heat treatment. The particles of coatings integrated with each other and the gap was filled.

Fig. 2(d) shows the microstructure of the coatings after 900 ℃ heat treatment. The structure is denser and has a more obvious mutual diffusion, especially at the boundary between the substrate and the coating. No unmelted particles were found in this figure.

Table 2 shows the results of the energy spectrum of different regions in Fig. 2(b). It is obvious that the granular and lath-shaped particles consist of pure metal. The coating cannot be deemed a HEA coating in zones A-D. Thus, it is hard to gain better wear or corrosion resistance in the as-sprayed coatings. However, at the bottom of the coating (Fig. 2(b)), five elements from the powders can be detected in region E. One explanation for this phenomenon is the heat preservation effect by the later deposited coatings. The heat preservation effect slowed down the cooling rate of the first-formed coating, which can be considered as a short-lived heat treatment. This short-lived heat treatment accelerated the element diffusion and preliminary formed a high entropy state in the coatings. Thus, the heat treatment should be used to gain a high entropy in the coating after the spraying process.

In Table 3, it can be seen that the elements in each particle have diffused after the vacuum heat treatment. The elements of coating after 900 ℃ were more homogeneous, according to Table 4.

Fig. 3 shows the map scanning results of the coating after heat treatment at 900 ℃. No HEA structure appeared after vacuum heat treatment.

Fig. 4 shows the coating morphology after laser re-melting. A molten pool was formed, which offers an opportunity for impurities (like oxides) to float up to the surface, and the pore was filled by molten metal. The molten pool reached the substrate, which can achieve metallurgical bonding instead of mechanical bonding. This result is similar to the conclusion of Yue et al. [29].

The phase structure of the re-melted coatings consists of a BCC structure and $AlNi_3$, according to the X-ray diffraction results. However, no $AlNi_3$ was ob-

Table 2
Energy spectrum analysis of different regions of as-sprayed coating

Zone	Fe/at.%	Co/at.%	Cr/at.%	Ni/at.%	Al/at.%
A	100	0	0	0	0
B	0	0	0	0	100
C	0	0	98.03	0	1.97
D	0.98	0	2.74	96.28	0
E	20.84	31.17	16.7	16.6	14.69

Table 3
Energy spectrum analysis of different regions of coatings after 600 ℃ heat treatment

Zone	Fe/at.%	Co/at.%	Cr/at.%	Ni/at.%	Al/at.%
A	65.09	0	17.61	0	17.29
B	41.06	15.33	43.58	0	0
C	14.75	0	0	85.25	0

Table 4
Energy spectrum analysis of different regions of coatings after 900 ℃ heat treatment

Zone	Fe/at.%	Co/at.%	Cr/at.%	Ni/at.%	Al/at.%
A	21.00	27.90	11.12	36.29	3.69
B	23.68	26.27	3.37	38.60	8.08
C	24.70	24.13	10.18	22.89	18.10
D	28.40	23.65	28.70	30.01	19.25

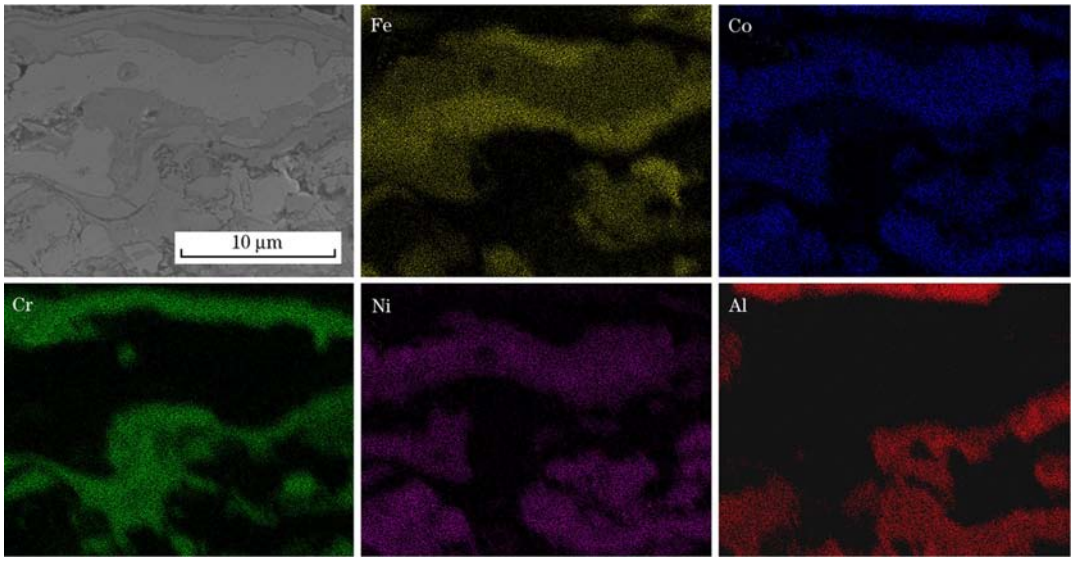

Fig. 3. Map scanning results of coating after 900 ℃ heat treatment.

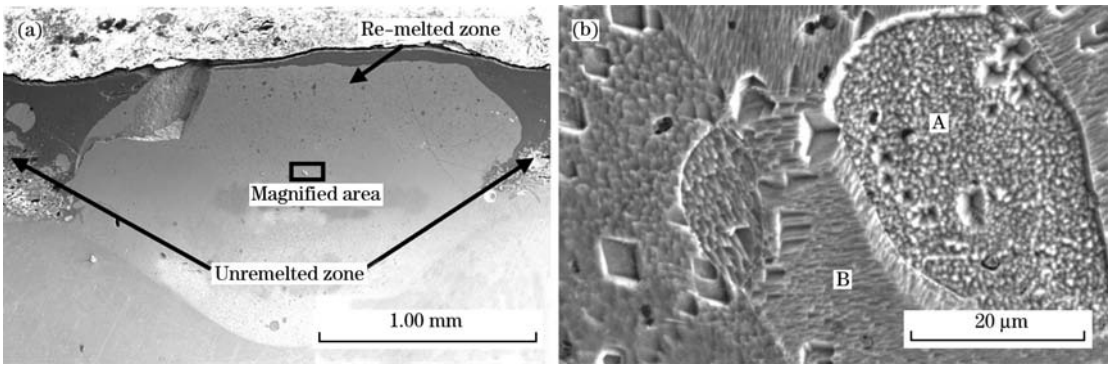

Fig. 4. Full view (a) and enlarged (b) structures of re-melted areas of coating after laser re-melting.

served by scanning electron microcopy. According to the analysis of the energy spectrum for the re-melted coating in Table 5, phases A and B were the same.

Table 5
Energy spectrum analysis of different regions of coatings after re-melting

Zone	Fe/at.%	Co/at.%	Cr/at.%	Ni/at.%	Al/at.%
A	31.62	16.25	14.85	20.58	16.70
B	30.51	15.99	15.03	22.82	15.65

As shown in Fig. 5, the elemental distribution was homogeneous after the re-melting procedure and no segregation exists. According to Eq. (2), the entropy reaches the highest point when the element is uniformly distributed. Thus, the laser re-melting procedure significantly enhanced the entropy.

Fig. 6 shows the hardness curve of coatings along the thickness direction. The average hardness of the as-sprayed coatings and coatings after vacuum heat treatment and laser re-melting were 177, 227, 266 and 682 HV, respectively. The vacuum heat treatment

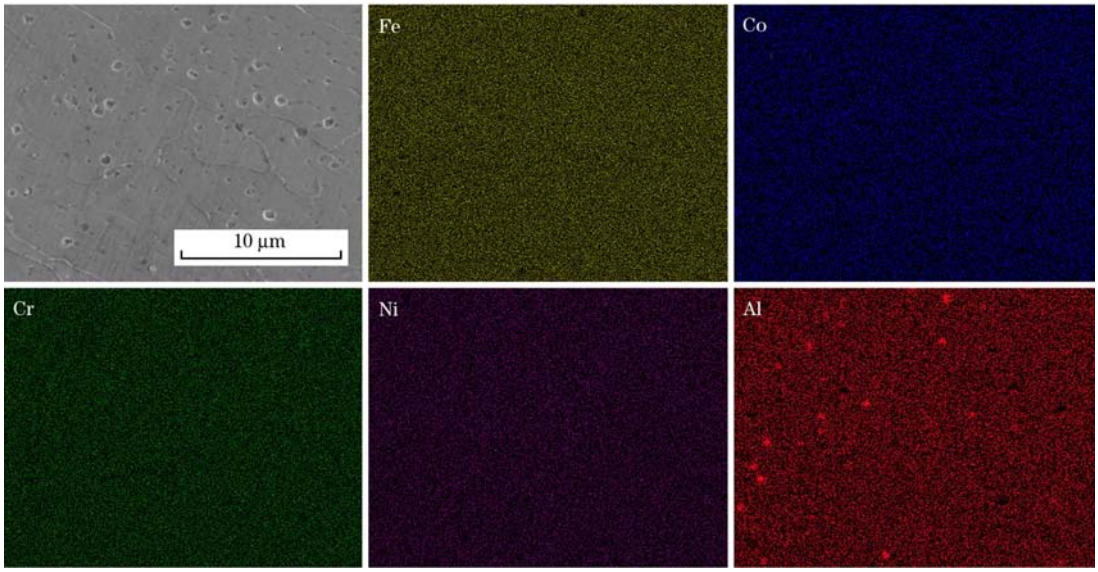

Fig. 5. Map scanning results of coating after laser re-melting.

and laser re-melting process have a significant impact on the hardness of the coatings. The hardness can be enhanced by increasing the heat treatment temperature.

During the heat treatment procedure, higher temperatures will enhance the extent of element diffusion. The element diffusion was uneven. Thus, some parts of the coatings present intermetallic compounds, which can enhance the hardness[30]. Other parts of the coating exhibited the high entropy, which decreased the free energy of coatings and restrained the formation of intermetallic compounds. As a result, solid solutions formed in these parts, which enhanced the hardness of the coatings by increasing the extent of lattice distortion and inhibiting dislocation motions.

The laser re-melting procedure has a more significant impact on the hardness of coatings. The homogeneous distribution of elements maximized the entropy, which increased the effect of high entropy to

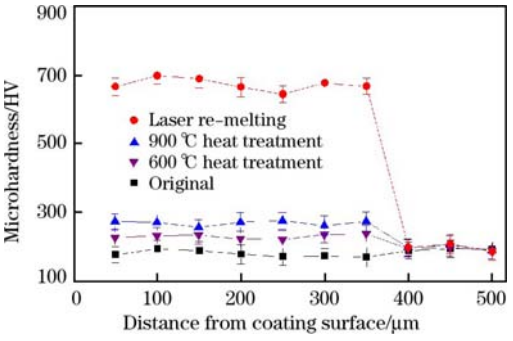

Fig. 6. Hardness curves of coatings treated with different processes.

the extent of maximum value in theory. As a result of this, only a single solid solution and $AlNi_3$ exist in the coating, which is better for increasing the hardness.

Fig. 7 shows the different surface morphologies of coatings after wear. The as-sprayed coatings show the worst wear resistance because of the low hardness and the non-existence of the wear resistance phase[31]. The worn mechanism was adhesive wear for the as-sprayed coatings. During the course of friction, the surface metal of coatings was exposed, since the oxidation film was rubbed away. The molecule between the two friction faces was bonded by intermolecular forces. With the friction process, the component of coatings flake from the surface, since the shear force at the friction face outweigh the support force of the coatings[32]. Thus, many pits exist at the surface of coatings after wear, as shown in Fig. 7(a).

Fig. 7(b) shows the surface structure after wear of coatings after 600 ℃ vacuum heat treatment. The wear resistance is better than that of the as-sprayed

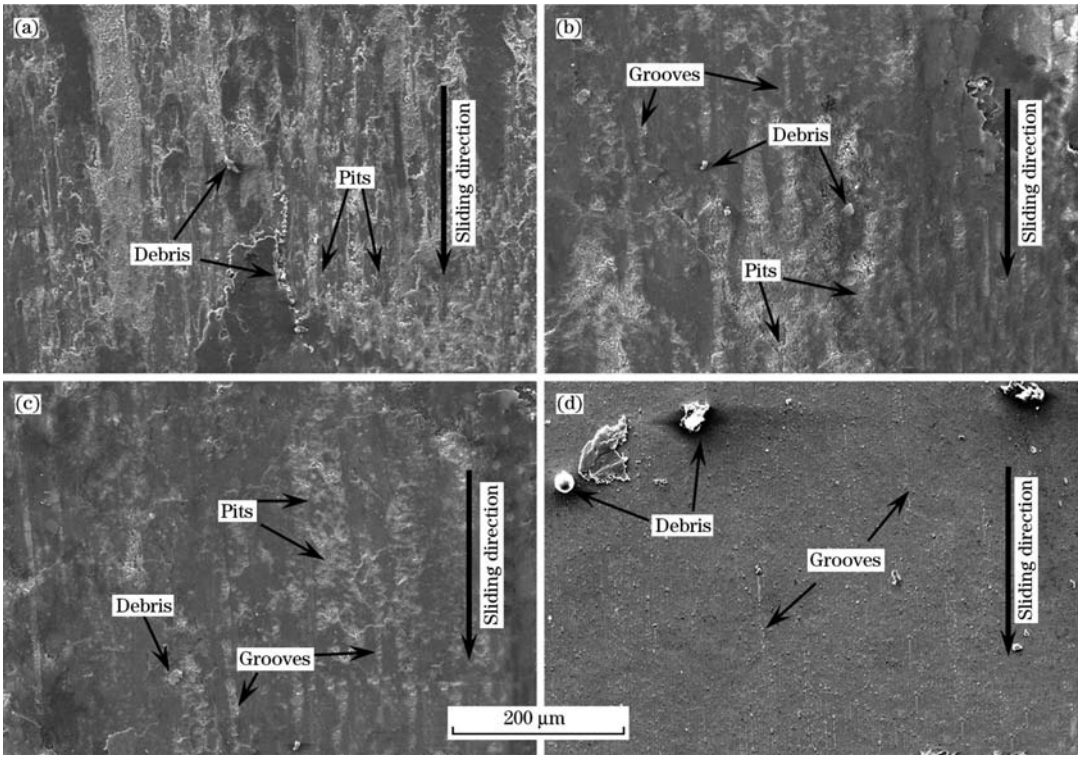

(a) As-sprayed coatings; (b) Coatings after 600 ℃ heat treatment; (c) Coatings after 900 ℃ heat treatment; (d) Laser re-melted coatings.

Fig. 7. Surfaces of coatings after wear.

coatings. It mixed adhesive wear and abrasive wear because both pits and grooves can be observed. The adhesive wear was relieved, since the hardness was increased by the vacuum heat treatment. The abrasive wear exists because of the formation of hard phases, like intermetallic compounds[33]. With increasing wear time, the metal binding phase was gradually reduced, which made the hard phases exposed. The hard phases fall off from the surface of the coatings and formed a new source of abrasive wear.

The wear resistance of coatings increased after 900 ℃ vacuum heat treatment, as shown in Fig. 7(c). It also consists of both adhesive wear and abrasive wear. However, the wear degree is slighter than 600 ℃, since the hardness has been improved.

After laser re-melting, the wear resistance is the best among all of the samples, which was similar with the results of Liu et al.[34]. The formation of intermetallic compounds was restricted by the effect of high entropy, which decreased the possibility of

abrasive wear.

The mass loss after wear is shown in Fig. 8. The wear resistance of the as-sprayed coating is the worst. With increasing heat treatment temperature, the coatings show better wear resistance. The coatings with laser re-melting show the best property of wear resistance, in accordance with the previous result.

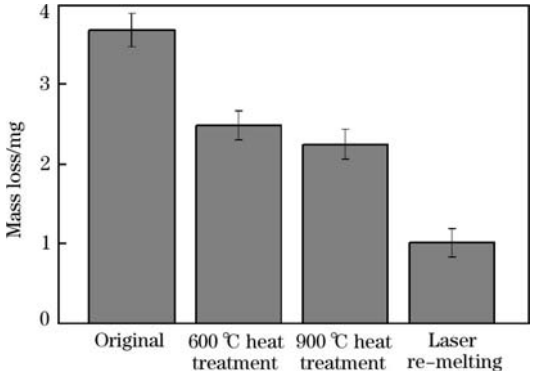

Fig. 8. Mass loss after treatment with different processes and temperatures.

4. Conclusions

(1) The as-sprayed coating mainly consists of pure metals. The vacuum hear treatment accelerated the alloying extent of the coatings and the BCC phase was formed.

(2) The alloying extent of coatings reaches its maximum value after laser re-melting. The intermetallic compound cannot be found due to the effect of high entropy except for $AlNi_3$, which has the lowest enthalpy of mixing. The metal atoms that cannot form an intermetallic compound and tend to form a supersaturated solid solution. This enhanced the coating hardness and wear resistance.

(3) The mass loss of the as-sprayed coatings is the largest after the wear test. The wear properties of coatings increased with increasing heat treatment temperature. The coatings after laser re-melting show the best wear resistance.

Acknowledgment

This work was financially supported by National Natural Science Foundation of China (Nos. 51301112 and 51401129), China Postdoctoral Science Foundation (2015M571327), the Natural Science Foundation of Liaoning Province (No. 201602553), and the Science Research Program of Education Department in Liaoning Province (No. L2014048).

References

[1] J. W. Yeh, Eur. J. Control 31 (2006) 633-648.
[2] J. W. Yeh, S. K. Chen, S. J. Lin, J. Y. Gan, T. S. Chin, T. T. Shun, C. H. Tsau, S. Y. Chang, Adv. Eng. Mater. 6 (2004) 299-303.
[3] J. W. Yeh, JOM 65 (2013) 1759-1771.
[4] Y. P. Lu, X. Z. Gao, L. Jiang, Z. N. Chen, T. M. Wang, J. C. Jie, H. J. Kang, Y. B. Zhang, S. Guo, H. H. Ruan, Y. H. Zhao, Z. Q. Cao, T. J. Li, Acta Mater. 124 (2017) 143-150.
[5] B. Gludovatz, A. Hohenwarter, D. Catoor, E. H. Chang, E. P. George, R. O. Ritchie, Science 345 (2014) 1153-1158.
[6] Y. J. Zhao, J. W. Qiao, S. G. Ma, M. C. Gao, H. J. Yang, M. W. Chen, Y. Zhang, Mater. Des. 96 (2016) 10-15.
[7] Y. Zhang, T. T. Zuo, Z. Tang, M. C. Gao, K. A. Dahmen, P. K. Liaw, Z. P. Lu, Prog. Mater. Sci. 61 (2014) 1-93.
[8] J. Qiao, H. Jia, P. K. Liaw, Mater. Sci. Eng. R 100 (2016) 1-69.
[9] L. S. Zhang, G. L. Ma, L. C. Fu, J. Y. Tian, Adv. Mater. Res. 631-632 (2013) 227-232.
[10] Y. P. Lu, Y. Dong, S. Guo, L. Jiang, H. J. Kang, T. M. Wang, B. Wen, Z. J. Wang, J. C. Jie, Z. Q. Cao, H. H. Ruan, T. J. Li, Sci. Rep. 4 (2014) 6200-6205.
[11] J. C. Qiao, J. M. Pelletier, N. Li, Y. Yao, J. Iron Steel Res. Int. 23 (2016) 19-23.
[12] Y. Zhang, J. W. Qiao, P. K. Liaw, J. Iron Steel Res. Int. 23 (2016) 2-6.
[13] S. Q. Xia, Z. Wang, T. F. Yang, Y. Zhang, J. Iron Steel Res. Int. 22 (2015) 879-884.
[14] X. T. Liu, W. B. Lei, J. Li, Y. Ma, W. M. Wang, B. H. Zhang, C. S. Liu, J. Z. Cui, Rare Metals 33 (2014) 727-730.
[15] B. Zheng, Q. B. Liu, L. Y. Zhang, Adv. Mater. Res. 820 (2013) 63-66.
[16] H. Zhang, Y. Pan, Y. He, J. Therm. Spray Technol. 20 (2011) 1049-1055.
[17] A. S. M. Ang, C. C. Berndt, M. L. Sesso, A. Anupam, S. Praveen, R. S. Kottada, B. S. Murty, Metall. Mater. Trans. A 46 (2015) 1-10.
[18] L. H. Tian, W. Xiong, C. Liu, S. Lu, M. Fu, J. Mater. Eng. Perform. 25 (2016) 5513-5521.
[19] P. Yang, Y. Liu, X. Zhao, J. Cheng, H. Li, Adv. Powder Technol. 27 (2016) 1128-1133.
[20] Q. S. Chen, K. Y. Zhou, L. Jiang, Y. P. Lu, T. J. Li, Arab. J. Sci. Eng. 40 (2015) 3657-3663.
[21] H. J. Park, Y. S. Na, S. H. Hong, J. T. Kim, Y. S. Kim, K. R. Lim, J. M. Park, K. B. Kim, Met. Mater. Int. 22 (2016) 551-556.
[22] D. Y. Lin, N. N. Zhang, B. He, G. W. Zhang, Y. Zhang, D. Y. Li, J. Iron Steel Res. Int. 24 (2017) 184-189.
[23] A. Takeuchi, A. Inoue, Mater. Trans 46 (2005) 2817-2829.
[24] M. Widom, Metall. Mater. Trans. A 47 (2016) 3306-3311.
[25] J. Lutz, D. Manova, J. W. Gerlach, M. Stormer, S. Mandl, IEEE Trans. Plasma Sci. 39 (2011) 3056-3060.
[26] D. Y. Dong, C. S. Liu, B. Zhang, J. Iron Steel Res. Int. 15 (2008) No. 3, 5-10.
[27] N. N. Zhang, D. Y. Lin, Y. L. Li, Y. Zhang, M. P. Planche, H. L. Liao, C. Coddet, F. Y. Dong, J. Iron Steel Res. Int. 24 (2017) 306-312.
[28] A. Munitz, S. Salhov, S. Hayun, N. Frage, J. Alloy. Compd. 683 (2016) 221-230.
[29] T. M. Yue, H. Xie, X. Lin, H. Yang, G. Meng, Entropy 15 (2013) 2833-2845.
[30] E. Svanidze, T. Besara, M. F. Ozaydin, C. S. Tiwary, J. K. Wang, S. Radhakrishnan, S. Mani, Y. Xin, K. Han, H. Liang, T. Siegrist, P. M. Ajayan, E. Morosan, Sci. Adv. 2 (2016) e1600319.
[31] C. P. Jiang, Y. Z. Xing, F. Y. Zhang, J. M. Hao, X. D. Song, J. Iron Steel Res. Int. 21 (2014) 969-974.
[32] Y. Liu, S. G. Ma, M. C. Gao, C. Zhang, T. Zhang, H. J. Yang, Z. H. Wang, J. W. Qiao, Metall. Mater. Trans. A 47 (2016) 3312-3321.
[33] R. Li, M. Wang, T. Yuan, B. Song, Y. Shi, Metall. Mater. Trans. A 47 (2016) 1-14.
[34] X. T. Liu, W. B. Lei, Q. J. Wang, W. P. Tong, C. S. Liu, J. Z. Cui, J. Iron Steel Res. Int. 23 (2016) 1195-1199.